ELECTRONIC STRUCTURE STUDIES OF THE C$_{60}$ FILM CONDENSED ON 2H-MoS$_2$(0001) SURFACE

Lu Hua(陆 华), Chen Ting(陈 挺)[†], Shen Dian-hong(沈电洪),

Bao Chang-lin(包昌林), Zhang Xiao-jun(张小军), Zhang Qing-zhe(张青哲),

Cui Yu-de(崔玉德), Xie Kan(谢 侃), Qian Sheng-fa(钱生法)[‡],

Wang Gang(王 刚)[‡], Xie Si-shen(解思深)[‡], and

Lin Zhang-da(林彰达)

State Key Laboratory for Surface Physics, Institute of Physics, Academia Sinica, Beijing 100080, China
[†]*Department of Physics, the Hong Kong University of Science and Technology,*
Clear Water Bay, Kowloon, Hong Kong
[‡]*Institute of Physics, Academia Sinica, Beijing 100080, China*

The electronic structure and vibrational spectrum of the C$_{60}$ film condensed on a 2H-MoS$_2$(0001) surface have been investigated by X-ray photoelectron spectroscopy (XPS), ultraviolet photoelectron spectroscopy (UPS), Auger electron spectroscopy (AES) and infrared high-resolution electron-energy-loss spectroscopy (HREELS). AES analysis showed that at low energy side of the main transition, C$_{60}$ contains a total of three peaks just like that of graphite. However, the energy position of the KLL main Auger transition of C$_{60}$ looks like that of diamond, indicating that the hybridization of the carbon atoms in C$_{60}$ is not strictly in sp^2-bonded state but that the curvature of the molecular surface introduces some sp^{2}p$_z$-bonded character into the molecular orbitals. XPS showed that the C 1s binding energy in C$_{60}$ was 285.0 eV, and its main line was very symmetric and offered no indication of more than a single carbon species. In UPS measurement the valence band spectrum of C$_{60}$ within 10 eV below the Fermi level (E_F) shows a very distinct five-band structure that characterizes the electronic structure of the C$_{60}$ molecule. HREEL results showed that the spectrum obtained from the C$_{60}$ film has very rich vibrational structure. At least, four distinct main loss peaks can be identified below 200 meV. The most intense loss was recorded at 66 meV, and relatively less intense losses were recorded at 95, 164 and 197 meV at a primary energy of electron beam $E_p = 2.0$ eV. The other energy-loss peaks at 46, 136, 157 and 186 meV in HREEL spectrum are rather weak. These results have been compared to infrared spectrum data of the crystalline solid C$_{60}$ taken from recent literatures.

PACC: 3640; 3365; 7320; 6855

I. INTRODUCTION

The existence of the isolated molecules of C$_{60}$ with a shape of truncated icosahedron with twenty hexagonal rings and twelve pentagonal rings was first discovered by Kroto, Smalley and coworkers.[1] In 1990, Kratschmer, Huffman and colleagues[2] invented techniques to produce and separate C$_{60}$ in sufficient quantity. Since then, experimental and theoretical studies on the physical and electronic properties of C$_{60}$ have developed extensively.[3] The electronic properties of the C$_{60}$ film have been examined using some electron spectroscopy[2,4–7] and

thought to be somewhat graphitic in character, with the sp^2-bonded sheets curved into a sphere. Theoretical studies[8] showed that the essence of the electronic properties of C_{60} is provided by σ-orbitals along the neighboring atoms and π-obitals extending outward from and inward to the cage. Each atom has one π-electron (filling the highest occupied level) and three σ-electrons. For C_{60}, the energy separation between the centers of the highest occupied molecular orbital (HOMO) and the lowest unoccupied molecular orbital (LUMO) derived bands is 3.75 eV[9−11], indicating that solid C_{60} would behave like a semiconductor.

Surface energy spectroscopic techniques, such as, AES, XPS, UPS and HREELS are powerful tools for the measurement of the electronic structures and the vibrational properties of solid surface. Because they have better sensitivity to the surface layer or the adsorbed molecular layer on solid surface, in recent years they have been used for the studies of the C_{60} film condensed on some semiconductor[4,11−23] and metal surfaces.[6,10,14,24−28] However, the information of the properties of the C_{60} film condensed on layered materials is still relatively less known, except in a few of papers[29−35] which introduced the epitaxial growth of C_{60} on the layered MoS_2, mica and GaSe surface, etc. In this paper, we report on the electronic-structures studies of C_{60} condensed on a cleaved 2H-MoS_2(0001) surface by surface-sensitive techniques, such as AES, XPS, UPS and HREELS. The natural MoS_2 single crystal with 2H stacking arrangement was chosen as a substrate material in our studies, because its cleaved (0001) surface exhibits the bulk semiconductor electronic bond structure[36], and it is also a layered material with weak van der Waals interlayer bonding, like graphite, in which all the orbitals in a plane are involved in bonding. The cleaved surface with a low surface energy has no dangling bonds, and large atomically flat areas can be easily obtained.

II. EXPERIMENTAL

AES experiment was performed on a Perkin Elmer model PHI-610 Scanning Auger Microprobe with single-pass cylinderical mirror analyzer (CMA) and coaxial electron gun ($0 < E_g < 10$ keV). The focussed electron beam ($3 \mu m^2$) can be scanned over the sample to obtain a secondary electron image of it. AES spectra were collected digitally in the $N(E)$ form and electronically differentiated. Data were analyzed in the differentiated form, $dN(E)/dE$. Depth profiling was performed with $1 - 2.0$ kV Ar^+ ions incident at about 45° with respect to the sample normal by alternately acquiring data and sputtering. X-ray photoelectron spectrum was recorded by an ESCALAB MK-II spectrometer of VG scientific Ltd. The system consists of two separately pumped chambers. The main analysis chamber is equipped with a non-monochromatized twin-anode (Al and Mg) radiation X-ray source with a microspot facility (from 150 up to 1000 μm diameter), a hemispherical analyser and a flood gun for charge neutralization. The ultraviolet photoelectron spectrum of the C_{60}

film was recorded with photon energy equal to 21.2 eV (He I). The pass energy was 2.0 eV, and the analyser resolution in the He I measurements was about 200 meV. All energy scales were referenced to the Fermi level (E_F) of the grounded substrate. HREELS measurements were performed in a Leybold-Heraeus ELS22 equipped with a low-energy electron diffraction (LEED) system. The background pressure was $\sim 5 \times 10^{-9}$ Pa. The HREELS spectra were recorded in the specular direction making an angle of 60° with the surface normal. The primary energy of electron beam E_p could be varied from 0 up to 20 eV. An attainable energy resolution is about 16 meV for infrared region. Prior to the measurement of the electronic and vibrational spectra, the substrate 2H-MoS$_2$(0001) surface and the C$_{60}$ films deposited on it with different thickness have to be subject to the low-energy electron diffraction (LEED) measurement. The clean 2H-MoS$_2$(0001) surface shows 1×1 LEED pattern, indicative of no major surface reconstruction under our experimental conditions. For the C$_{60}$/2H-MoS$_2$ system, unless the coverage of C$_{60}$ is very low (< 3 monolayers), the LEED patterns can be observed; while in the case of thick films, no LEED patterns could be seen, indicating the thick C$_{60}$ films condensed on MoS$_2$ at room temperature are disordered or clumped in islands. The growth of C$_{60}$ on the 2H-MoS$_2$(0001) surface was carried out in an evaporation chamber with a background pressure of 1×10^{-8} Pa. The purified C$_{60}$ powders (99.90%) (supplied by the Group of Nano Materials and Physics, Institute of Physics, Academia Sinica, China) were charged in a tantalum boat. A 2H-MoS$_2$ single crystal substrate was cleaved in air just before loading into the evaporation chamber, and then cleaned by heating at 200–250°C under the ultra high vacuum until a sharp (0001)1×1 LEED pattern was displayed. The substrate was then positioned within the flux of material to be deposited 1.5 cm from the face of the boat. To initiate the growth, the Ta boat charged with C$_{60}$ powders was heated in ultra high vacuum by its own electric resistivity at 250°C, for 1h for outgassing. The C$_{60}$ was then sublimed at a pressure of 3×10^{-7} Pa at 300°C on to the clean 2H-MoS$_2$(0001) surface. The typical deposition rate was about 0.09 nm·min^{-1}. We define one monolayer (ML) of C$_{60}$ to be the equivalent of 1.156×10^{14} molecules·cm^{-2}. The thickness per layer is 0.8 nm based on the bulk density of 1.65 g·cm^{-3} and the layer spacing for a close-packed solid.

III. RESULTS AND DISCUSSION

A. Auger electron spectroscopy (AES)

The electron-excited C$_{KLL}$ Auger spectra were collected in the pulse-counting mode in order to maximize spectral resolution and then differentiated numerically. Figure 1 is the Auger spectrum obtained from the clean 2H-MoS$_2$(0001) surface. It can be seen clearly that

there is not any carbon or oxygen contaminant on the surface. The KLL Auger spectrum
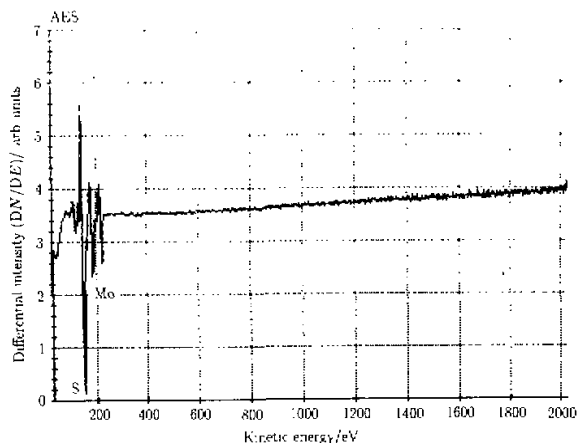obtained from the C_{60} film with about 4.6 ML in thickness condensed on the 2H-MoS$_2$(0001)

Fig. 1. Auger spectrum of the clean 2H-MoS$_2$(0001) surface.
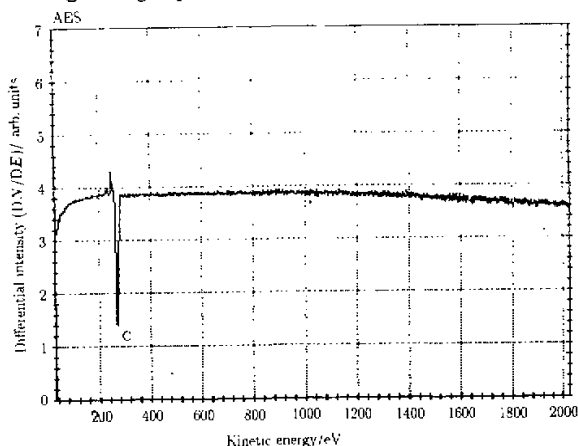

Fig. 2. C_{KLL} Auger spectrum of the C_{60} film with 4.6 ML
in thickness condensed on the 2H-MoS$_2$(0001) surface.

surface at room temperature is showed in Fig. 2. The line shape and the fine structure are
very similar to that of graphite. Because the detail of C_{KLL} line shape is very sensitive to
the hybridization of the carbon atoms and thus to the allotropic nature of the films, we
illustrate a comparison of the fine structures of C_{KLL} Auger spectra taken from the three
different carbon allotropes (C_{60}, graphite and diamond) in Fig. 3. It is evident that at the
low energy side of the main transition, C_{60} contains a total of three peaks (same as graphite),
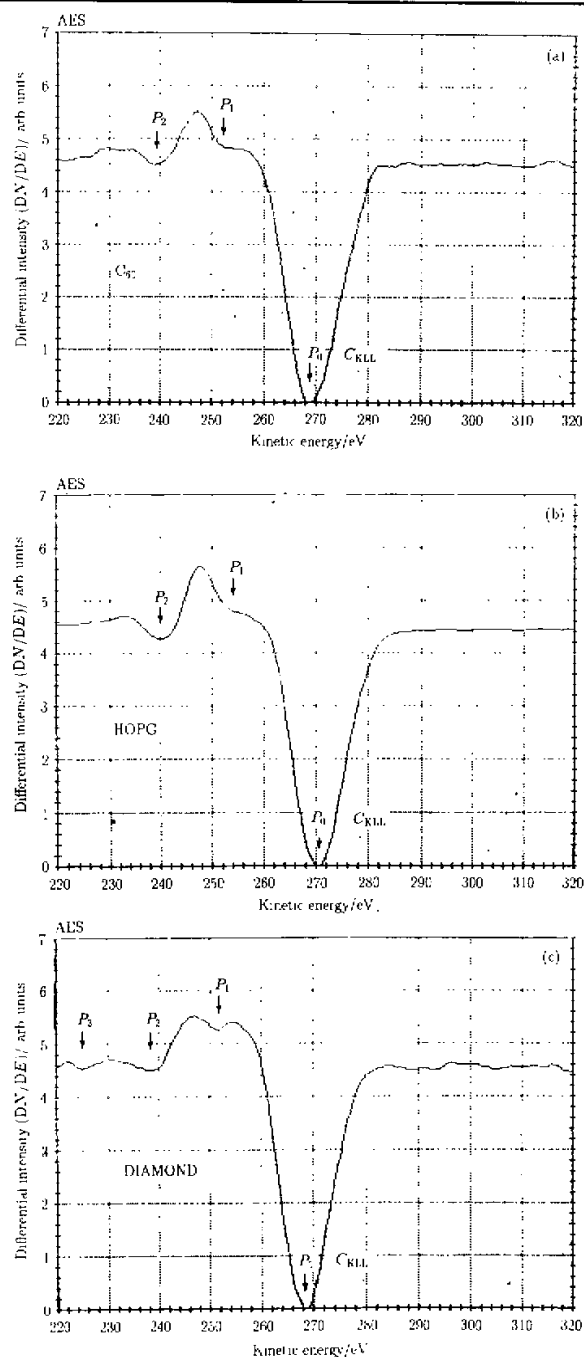while diamond has four peaks. But, there is a small shift toward the lower kinetic energy

Fig. 3. Comparison of the fine structure of C_{KLL} Auger spectra taken from the three carbon allotropes: (a) C_{60}, (b) graphite and (c) diamond.

direction in the whole of the peaks of C_{60}. It may be caused by the charging effect on the surface of the insulating C_{60}. Considering the predictions from the band model for KVV Auger transitions[37,38], we can discuss the origin of the difference of the Auger fine structures in different allotropes of carbon. For the main Auger peak P_0 (the positions of the Auger peaks taken in the derivative curve are represented by the single of $P_n(n = 0, 1, 2$ and 3)), if the electron originates in the valence band, we have a simple expression[39]

$$E_a = E_c(Z) - 2V ,$$

where E_a is the energy of the Auger electron relative to the Fermi level of the specimen, $E_c(Z)$ is the binding energy of c shell electron of Z element, and V represents the energy of a prominent feature in the valence band of the specimen. Applying this formula to carbon, using the values of atomic binding energies published by Bearden and Burr[38] ($E(Z) = 283.8$ eV for carbon) and those of the theoretical density of states in valence bands
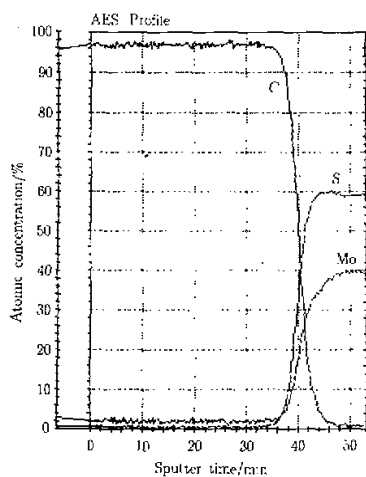

of the three species of carbon, we have calculated the Auger peak energy, and identified the transition of the Auger electrons. In the calculated energy item, the theoretical densities of states for diamond and graphite refer to the band structure of Painter[40] and Willis[41] (also see Ref.[39]), while that for C_{60}, it refers to the UPS data in this work. The energy of the plasma oscillation of the valence electrons in the free-electron model is given by[42]: $E_p = \hbar\omega_p$, and $\omega_p = \sqrt{(4\ ne^2/m)}$, where n, e and m are electron density, charge, and mass, respectively. Assuming four valence electrons per carbon atom, we can obtain a set of values for the plasmon energy; that is, the E_p's (bulk plasmon) are equal to 21.5, 31.2 and 14.5 eV for C_{60}, diamond and graphite respectively. In the same approximation the energy of the surface plasmon is given by[42]: $E_s = \hbar\omega_s = \hbar\omega_p/\sqrt{2}$, therefore the E_s's (surface plasmon) are equal to 15.2, 22.1 and 10.2 eV for C_{60}, diamond and

Fig. 4. Auger electron depth profile of the C_{60} film with about 25 nm in thickness condensed on the 2H-MoS_2(0001) surface.

graphite respectively. Table 1 illustrates the position and identification of the fine structure in the C_{KLL} spectra from the three allotropes: C_{60}, graphite (HOPG) and diamond. The difference in Auger fine structures reflects the difference in band structures. And, we can assign the observed Auger peaks P_0 (268.5 eV) in C_{60} to KV_4V_4 Auger transition. While the two additional peaks on the low-energy side of the main Auger transition, the P_1 (252 eV) and P_2 (239 eV) may be corresponding to the plasma oscillation peaks. The solid C_{60} differs from diamond or graphite in a fundamental way related to the hybridization of the atomic s- and p-levels. In diamond, sp^3 hybridization assures a bond angle of 109°28′ and four identical bonds. In graphite, sp^2 hybridization produces three equivalent bonds, a bond angle of 120°, and strong planar bonding. The out-of-plane p orbitals result in π-bonds

Table 1.   Peak position and identification of the fine structure in the C_{KLL} spectra from three allotropes: C_{60}, Graphite (HOPG) and Diamond.

		Peak energy /eV	Peak position relative to P_0 /eV	Calculated energy[*] /eV	Identification
C_{60}	P_0	268.5		268.7	KV_4V_4
	P_1	252.0	16.5	253.3	$P_0 - \hbar\omega_s$
	P_2	239.0	29.5	238.1	$P_0 - 2\hbar\omega_s$
HOPG	P_0	270.5		270.8	KV_2V_1
	P_1	254.0	16.5	253.8	KV_4V_3
	P_2	240.0	30.5	241.5	$P_0 - 2\hbar\omega_p$
diamond	P_0	268.5		268.4	KV_3V_2
	P_1	252.0	16.5	252.4	KV_3V_2
	P_2	238.0	30.5	237.3	$P_0 - \hbar\omega_p$
	P_3	225.0	43.5	224.3	$P_0 - 2\hbar\omega_s$

[*] The theoretical density of states for diamond and graphite refers to the band structure of Painter[40] and Willis[41], while for C_{60}, it refers to the UPS results in this work.

and weak interplanar bonding. In comparison, the energy position of the C_{KLL} main Auger transition of C_{60} is much the same as that of diamond, while the peak shape looks like that of graphite, indicating that the hybridization of the carbon atoms in C_{60} may be not strictly in sp^2-bonded manner but that the curvature of the molecular surface introduced some sp^2p_z-bonded character into the molecular orbitals, as discussed by Haddon et al.[43] They suggested that the hybridization of the s-and p-orbitals in C_{60} is an intermediate between pure sp^3 and sp^2p, introducing a pyramidalization angle of $11.6°$ for C_{60}. The solid C_{60} is characterized as a molecular crystal. As such, their orbitals are modified, but not too seriously, by condensation to form solid films. Figure 4 is the Auger electron depth profile of the C_{60} film with about 25 nm in thickness condensed on the 2H-MoS$_2$(0001) plane. It can be seen from Fig. 4 that there is no strong interfacial reaction at room temperature although we can see an interface diffusion region with about 5 nm in broadness. We consider it to be due to the fact that layered 2H-MoS$_2$ surface has no dangling bonds.

B. X-ray photoelectron spectroscopy (XPS)

Figure 5 shows the XPS spectrum of molybdenum and sulphur core level transitions in the clean 2H-MoS$_2$(0001) surface with MgKα radiation ($h\nu = 1253.6\,eV$). The results showed that the surface contamination peaks of carbon and oxygen were almost below the noise level. And the peaks of Mo3d ($3d_{5/2} = 229.5\,eV$; $3d_{3/2} = 232.7\,eV$) and S2p ($2p_{3/2} = 162.5\,eV$) can be identified clearly. The Mo($3d_{5/2}$)-S($2p_{3/2}$) binding energy difference at 67.0 eV is in excellent agreement with that reported in Ref.[44]. The X-ray photoelectron spectrum of the C_{60} film condensed on the clean 2H-MoS$_2$(0001) surface has also been recorded. After deposition of C_{60}, the XPS spectrum (Fig. 6(a)) showed that the C1s binding energy in C_{60} is 285.0 eV, and its main line is symmetric and offers no indication of more than a single
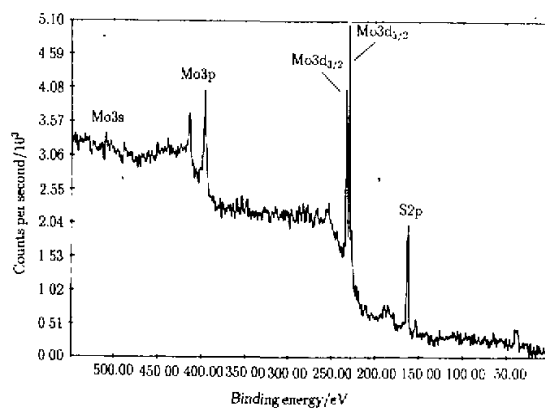
Fig. 5 XPS spectrum of Mo and S core level transitions in the clean $2H\text{-}MoS_2(0001)$ surface with $h\nu = 1253.6\,eV$.
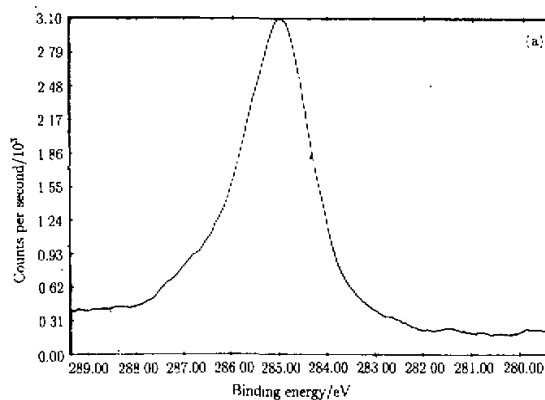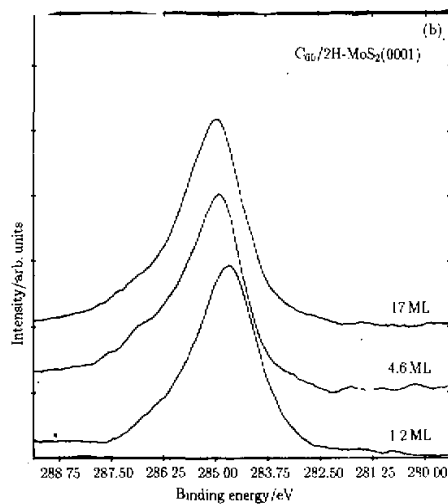

Fig. 6(a) XPS spectrum of the C_{60} film. The C1s binding energy is $285.0\,eV$. (b) Change of the binding energy and the C1s line shape with the C_{60} film thickness.

carbon species. Figure 6(b) shows that there are small changes in C1s binding energy and its line shape changes with increasing thickness of C_{60} film. A shift of 0.31 eV toward the higher binding energy side and the broader line shape on base can be seen clearly. The symmetry becomes better with the increase of the thickness; as the film thickness is more than 5 ML, these changes can be observed no longer. It indicates that very weak interface reaction between C_{60} and the sulfur layer of the 2H-MoS_2(0001) surface may exist in the early stage of the film deposition. This suggestion is consistent with the AES profile analysis. Figure 7 illustrates a comparison of C_{60} with the major Csp^3-hybridized diamond and Csp^2-bonded graphite in the XPS spectra of the C1s regions. The binding energies of the C1s peaks, referenced to E_F, are 285.0, 284.5 and 284.2 eV for C_{60}, diamond and graphite respectively. There is a 0.8 eV shift toward the high binding-energy side, relative to that in graphite. Moreover, the peak shape of the C1s in graphite was broader than that in C_{60}, which is consistent with the asymmetric of the XPS main line shape of a conductor. The C1s peak in C_{60} is more symmetric, as is usually so for an insulator diamond.[45]
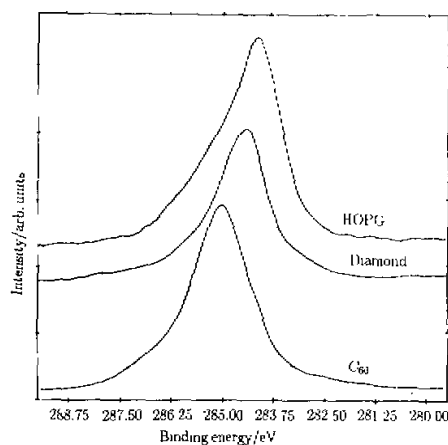

Fig. 7. Comparison of C_{60} with diamond and graphite in XPS spectra of the C1s regions.

C. Ultraviolet photoelectron spectroscopy (UPS)

UPS was used to measure the positions and line shape features of the valence band of the substrate 2H-MoS_2 and the C_{60} films. Figure 8 shows the spectrum of UPS (He I, $h\nu = 21.2$ eV) for the valence band structure of the clean 2H-MoS_2(0001) surface, the energy levels are aligned to E_F. The positions of the four main peaks in our UPS spectra were in agreement with those in previous studies.[36,46] Peak A (-2.7 eV) was believed to be mainly due to nonbonding $4d_z$ electrons, while peaks B (-4.25 eV), C (-5.8 eV) and D (-7.15 eV) were attributed to Mo(4d)–S(3p) bond in which S3p electrons were predominant. The valence-band spectrum of the C_{60} film with 4.6 ML thickness condensed on the 2H-

$MoS_2(0001)$ surface is shown in Fig. 9. It provides an overview of the distribution of the states for C_{60}, showing the full valence bands within 10 eV below E_F. The photoemission spectra were obtained using He I with a resolution of 200 meV. A very distinct five-band
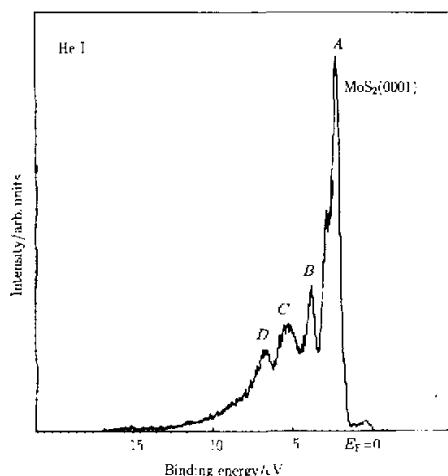

Fig. 8. UPS spectrum for the valence band structure of the clean 2H-$MoS_2(0001)$ surface at $h\nu = 21.2$ eV, the energy levels are aligned to E_F.
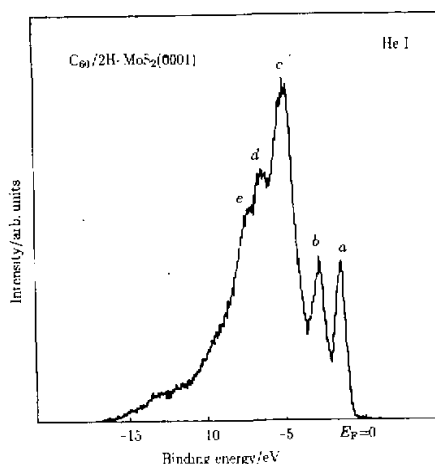

Fig. 9. Valence-band spectrum of the C_{60} film condensed on the 2H-$MoS_2(0001)$ surface. The film thickness is 4.6 ML.

-2.55 eV; V_2 at -3.95 eV; V_3 at -6.0 eV; V_4 at -7.55 eV and V_5 at -8.4 eV) can be identified clearly, which characterizes the electronic structure of the C_{60} molecule. Comparing with the calculations of the density of states (DOS) for solid C_{60}[47], we found that the $C2p_\pi$ levels fall within 5 eV below E_F, the $2p_\sigma$ levels are concentrated between 5 and 10 eV, and
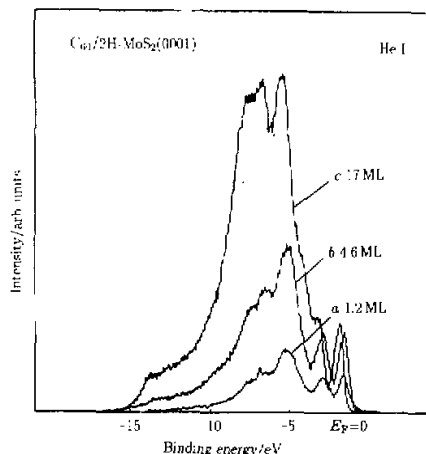
Fig. 10. Comparison of the UPS spectrum line for the C_{60} films in different thickness. Curves $a - c$ correspond to 1.2, 4.6 and 17 ML, respectively.

the deeper states are derived from 2s-derived σ-bands[4,6,47−49]; p-states are dominate at low energy, and s-states are stronger at higher energy. We note that charging effects may be important for thick films, because of the high intrinsic resistivity of C_{60}. Such effects would introduce a little shift to the higher energy side relative to E_F. Our studies on the C_{60} films with different thicknesses showed that on increasing the thickness of the C_{60} films from 4.6 to 17 ML, the energy position of the peaks shifts about 0.3 eV toward the higher binding energy side (see Fig. 10). Moreover, the relative intensity of the peaks (s-states, at higher energy) appears a great increase, indicating that the charging effects exist at least for the C_{60} films with a thickness of more than 4.6 ML. We cannot rule out that the change might be due to symmetry reduction in the C_{60} molecules in the vicinity of the surface of the thick C_{60} film, but the disorder effects in the growth of C_{60} films or some weak interface reaction between C_{60} and the substrate may be also important for the measurement of the valence-band spectra. The overall valence-band structure is very analogous to that of graphite or diamond, but the molecular symmetry of C_{60} assures sharp spectral features.

D. High-resolution electron-energy loss spectroscopy (HREELS)

HREELS is a far more surface-sensitive spectroscopy than XPS or UPS to examine the energy of vibrational modes of film on solid surface. According to the semiclassical dielectric theory, the probing depth of the HREELS turns out to be at least 10 nm[19]. Figure 11 shows the infrared energy loss spectrum of the clean 2H-MoS_2(0001) substrate in a range of 0–200 meV (1 meV=8.06 cm^{-1}) obtained at a primary electron beam energy (E_p) of 5 eV. In the surface layer of 2H-MoS_2(0001) there are three atoms per unit cell, so nine modes are
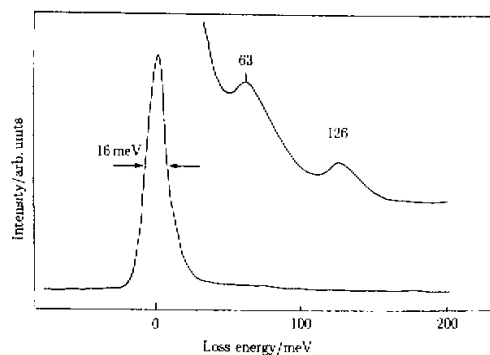
Fig. 11. HREELS spectrum of the clean 2H-MoS$_2$(0001) surface, $E_p = 5.0$ eV.
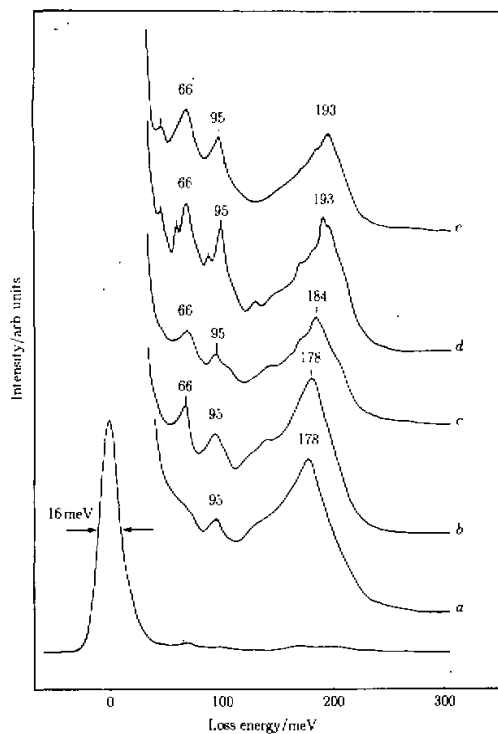
Fig. 12. HREELS spectrum of the C$_{60}$ films condensed on the 2H-MoS$_2$(0001) surface. The films from 0.58 to 8.07 ML are deposited at room temperature. $E_p = 5.0$ eV. Curves $a - e$ correspond to 0.58, 1.73, 5.19, 6.34 and 8.07 ML, respectively.

expected: three acoustic and six optical modes. The point group for the surface is C_{3v}, there will be three A_1 modes and three doubly degenerate E modes.[50] However, only two distinct peaks can be seen. One is the vibration of the dipole-active optical phonons, near

63 meV (508 cm^{-1}), which is assigned to one of the strongly active MoS$_2$ optical phonons, although its width is larger than those of the phonon-excitation loss peaks; and the other is an overtone of the vibrations, which can be observed at twice the phonon energy, but are low in intensity. Figure 12 shows the HREELS spectra of the C$_{60}$ films evaporated on the clean 2H-MoS$_2$(0001) surface with different thicknesses from 0.58 to 8.07 ML. The E_p was 5 eV, with its peak position estimated to be ±0.2 meV. The molecular vibrations span the energy range of 0–300 meV. Because the elastic peak has been broadened somewhat of its energy distribution (16 meV), it is not sufficient for identifying the very fine vibrational structure in HREEL spectrum. In the case of 0.58 ML C$_{60}$ film (curve a in Fig. 12), the original two peaks at 63 meV (508 cm^{-1}) and 126 meV (1016 cm^{-1}) observed from MoS$_2$ surface disappeared, while two new peaks at 95 meV (766 cm^{-1}) and 178 meV (1435 cm^{-1}) occurred. On increasing the C$_{60}$ film thickness to 1.73 ML (curve b in Fig. 12), a peak at 66 meV (532 cm^{-1}) appeared. It can be assigned to the expected surface phonon mode, which is optical and will be dipole-active vibrations. When the thickness of C$_{60}$ film reached 5.19 ML three main loss peaks and several weak emission signals could be identified below 200 meV (curve c in Fig. 12). The most intense loss was recorded at 184 meV (1483 cm^{-1}) which had a shift of 6 meV toward the high energy side, and relatively less intense losses were recorded at 66 meV (532 cm^{-1}) and 95 meV (766 cm^{-1}). However, when the thickness of the C$_{60}$ film was increased to 6.34 ML, (curve d in Fig. 12), a blue-shift of ~15 meV from 178 meV (1435 cm^{-1}) to 193 meV (1556 cm^{-1}) occurred evidently. The other six energy-loss peaks around these main peaks in HREEL spectrum were rather weak. Since C$_{60}$ is insulating, very thick film of C$_{60}$ is not suitable for HREELS analysis, which requires either conducting surfaces or sufficiently thin films on conducting substrates to reduce the charging effects. Curve e in Fig. 12 shows that in the case of 8.07 ML thick C$_{60}$ film, only three distinct loss peaks can be identified. Several weak losses do not appear in the HREEL spectrum of thick film of C$_{60}$. However, an increase in the background intensity and a decrease in the elastic line absolute intensity are observed. And the energy resolution is reduced. It is due to that most of the thick films of C$_{60}$ deposited at room temperature are generally disordered and show charging effect. Figure 13 shows the line shape of the main energy-loss peaks in HREELS spectrum as a function of incident electron beam energy, E_p. As can be seen, on reducing the E_p from 5.0 down to 4.5 eV, the HREELS spectra show no changes, namely, the spectra retain the characteristic features, three main peaks at 66 meV (532 cm^{-1}), 95 meV (766 cm^{-1}) and 193 meV (1556 cm^{-1}) and several weak peaks can be identified. When E_p is reduced to 2.0 eV, the vibrational spectrum features of the C$_{60}$ film exhibit a greater variation in intensity as a function of photon energy, for example, the 66 meV (532 cm^{-1}) loss peak increases evidently, and the 193 meV (1556 cm^{-1}) loss peak splits into two peaks at 164 meV (1322 cm^{-1}) and 197 meV (1588 cm^{-1}) and several

weak loss peaks around them. These variations reflect the unique molecular symmetry of C_{60}, and the normal modes in C_{60} above $800\,cm^{-1}$ involve atomic displacements that are predominantly tangential displacement of carbon atoms along the ball surface.[51] With continuously decreasing E_p to $1.5\,eV$, the spectra show no evident changes, but some small peaks disappears. At $E_p = 1.0\,eV$, the change mentioned above no longer occurs. It is well

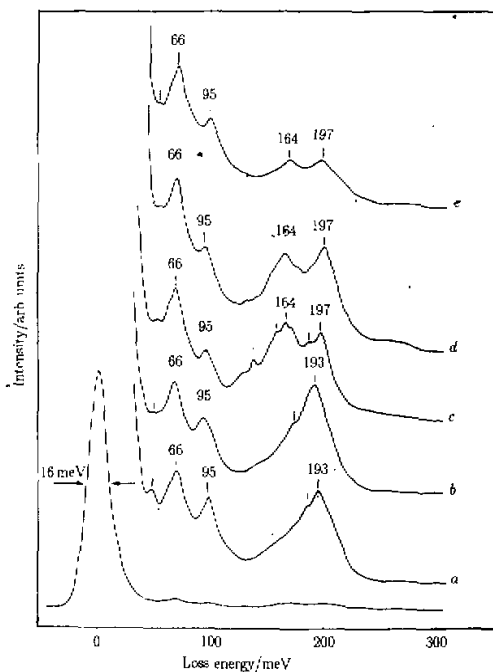Fig. 13. Line shape of the main energy loss peaks in HREELS spectrum as a function of E_p.
Curves $a - e$ correspond to 5.0, 4.5, 2.0, 1.5 and 1.0 eV, respectively.

known that in the infrared study the spectrum is dominated by the electron-dipole active modes which present a component of the transition dipole moment perpendicular to the surface. The reason is that the dipole selection rule plays a key role in mode assignment and adsorption site determination for polyatomic molecules. However, as pointed out by Weaver[11] in his paper on electronic structure of C_{60} that the first two valence band features for solid C_{60} have π_u and π_g character with 5-fold and 9-fold degeneracy, respectively. In photoemission, therefore, the relative emission intensities from the π_u and π_g bands change with photon energy because of matrix elements effects. Thus, we consider that in HREELS measurement the change of intensities of the loss peaks with incident electron beam energy (E_p) may also be due to the matrix elements effects. Because, in general, the spectra acquired with low-energy electrons emphasize the π-states of C_{60} over the σ-states. If it is true, we

suggest the importance of dipole transitions and the retention of molecular symmetry in a broad infrared bands. That may be one of the reasons why the loss peak at 193 meV ($1556\,cm^{-1}$) splits into two new peaks at lower E_p. There are 174 intramolecular vibrational modes for a 60 C-atoms molecules (3N-6), but under I_h symmetry[1] only 14 of the 46 distinct eigenvalues (see Table 2) are allowed in the infrared and the Raman spectra. The four infrared active modes have T_{1u} symmetry and are triply degenerate, the Raman active modes consist of two singly degenerate A_g modes and eight five-fold degenerate H_g modes.[52−56] With reference to the relations between the structural symmetry and the eigenfrequencies of C_{60}, in comparison to the infrared spectrum[54] and the Raman spectrum[56] of crystalline solid C_{60}, we see that the dipole-active modes identified in our HREELS spectrum from a thick C_{60} layer (curve c in Fig. 13) at 66 meV ($532\,cm^{-1}$), 95 meV ($766\,cm^{-1}$), 164 mev ($1322\,cm^{-1}$) and 197 meV ($1588\,cm^{-1}$) do not exactly match the four intense infrared bands at 527, 576, 1182 and $1429\,cm^{-1}$. The

Table 2.   The number of distinct vibrational eigenvalues and degeneracies of C_{60}[54].

I_h group label	Number of eigenvalues	Degeneracy	
A_g	2	1	
T_{1g}	3	3	
T_{3g}	4	3	even parity
G_g	6	4	
H_g	8	5	
A_u	1	1	
T_{1u}	4	3	
T_{3u}	5	3	odd parity
G_u	6	4	
H_u	7	5	

66 meV ($532\,cm^{-1}$) peak corresponds to the two of the four strongest infrared adsorption spectroscopy lines with T_{1u} dipole-active modes at 527 and $576\,cm^{-1}$, which are too close to be resolved in our HREELS results without further processing of the data. The 66 meV ($532\,cm^{-1}$) loss energies can be assigned to the same modes responsible for infrared absorption at $527\,cm^{-1}$ with a blue-shift of $5\,cm^{-1}$. The other three peaks at 95 meV ($766\,cm^{-1}$), 164 meV ($1322\,cm^{-1}$) and 197 meV ($1588\,cm^{-1}$) are likely to correlate better with dipole-inactive Raman lines than with the other two weak infrared lines at 1182 and $1429\,cm^{-1}$. As reported by Oshima *et al.*[57], in the angle-resolution EELS spectrum of the graphite (0001) surface there are large densities of vibrational states around 55, 90–100, 155 and 180 meV. Except for the peak at 55 meV, these energy losses correspond to our three C_{60} characteristic peaks, as if the C_{60} retains most of the vibrational features of graphite when we consider the "buckyball", C_{60}, being warped from graphitic sheet. It is because the electronic density in the π- and σ-orbitals is not changed significantly when planar graphite is curved to form

a C_{60}. Relatively weaker losses can also be seen from curve c in Fig. 13. But it is difficult at this point to know which modes are responsible for the observed vibrational spectra because these weaker vibrations may consist of two parts, in one of which the molecules make translation, i.e., the translational lattice modes, and in the other part the molecules rotate, i.e., the librational lattice modes. The translational lattice modes are of ungerade symmetry for the C_{60} structure, hence one expects these modes to be only infrared active. The librational modes are of gerade symmetry, and thus are expected to be Raman active. Some data taken from recent literatures[18,24,35] are illustrated in Table 3 for comparison of the C_{60}/2H-MoS$_2$(0001) HREELS spectrum with those of C_{60}/Si(100), C_{60}/GaSe(0001) and C_{60}/Rh(111) systems. We note that although GaSe and MoS$_2$ are all layered materials, the feature and position of the energy loss peaks in the C_{60}/GaSe system are different from those in the C_{60}/2H-MoS$_2$ system. It is due to the fact that MoS$_2$ is completely covalent

Table 3. Comparison of the C_{60}/2H-MoS$_2$(0001) HREELS spectrum with that of C_{60}/Si(100), C_{60}/GaSe(0001) and C_{60}/Rh(111) system.

Infrared modes*[54]		Raman modes*[56]		C60/2H-MoS2(0001) Ep=2.0 eV		C60/GaSe(0001)[35] Ep=3.7 eV		C60/Si(100)[18] Ep=3.7 eV		C60/Rh(111)[24] Ep=2.0 eV	
meV	cm⁻¹	meV	cm⁻¹	meV	cm⁻¹	meV	cm⁻¹	meV	cm⁻¹	meV	cm⁻¹
		34	272								
		54	432								
		61	495								
65	527			66	532	66	532	66	532	68	548
71	576					72	580				
		88	710								
		96	772	95	766			94	758	96	770
		136	1100								
147	1182					147	1185				
		155	1249	164	1322			156	1257	151	1215
		177	1425								
179	1429					178	1435				
		182	1468							183	1474
		195	1574	197	1588			194	1564		

*Crystalline solid C_{60}.

bonding within its layers, unlike GaSe which is partly ionic and has infrared active lattice vibrations. As mentioned above, in MoS$_2$ there are no dangling bonds on either the molybdenum or the sulfur surface atoms, the "lone pairs" of S3s electrons occupy very stable orbitals. The undisturbed (0001) basal plane surface of the 2H-MoS$_2$ has been proved to be inert, and it has no capability of forming strong bonds unless its molecular orbitals scheme is altered by physical or chemical manipulation. Why, then, except for the peak at 66 meV (532 cm^{-1}) the rest of the spectrum in C_{60}/2H-MoS$_2$(0001) system look like the case in C_{60}/Si(100) system? Possibly, it is due to the existence of defects, specifically the sulfur vacancies in MoS$_2$ within the basal plane or at step sites on the basal surface. The vacancies

might act as anchor sites where substrate atoms could bond directly, or they might serve as sites where atoms are substituted to form bridge bonds between substrate and film atoms. In this case, the deposition of C_{60} onto the cleaved 2H-MoS$_2$(0001) might have a greater effect on the Mo3d core levels than on the S2p levels. The photoemission studies[12] have revealed that the first-layer C_{60} bonding to the substrate surface is more than simply van der Waals in character. In order to compensate the differences in work functions, a dipole layer is formed at the interface. Such dipoles reflect mixing of the empty π-states of the C_{60} molecules with states of the substrate, yielding a π-resonance. For the sake of discussion on the chemical reactivity between C_{60} and 2H-MoS$_2$ surface, knowing their level s near the Fermi level is indispensable. These levels for 2H-MoS$_2$ and C_{60} are shown in Fig. 14, where the Fermi level for MoS$_2$ is –5.2 eV[58], and the band gap between the conduction band minimum (CBM) and the valence band maximum (VBM) is 1.35 eV[59], which is primarily due to a strong hybridization of the Mo 4d-bands and S5s-bands. The 5-fold degenerate HOMO, H_u, are separated from the 3-fold degenerate LUMO, T_{1u}, by a ground state energy gap of
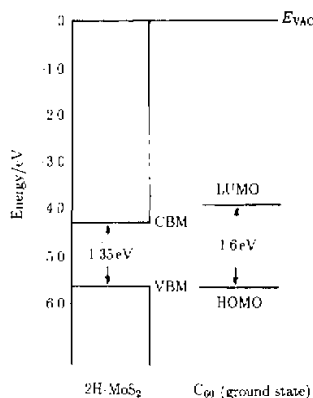

Fig. 14. Energy-level diagram for C_{60} condensed on the 2H-MoS$_2$(0001) surface, assuming vacuum level alignment.

and the center of the HOMO-LUMO gap of C_{60} is –4.8 eV.[12] Figure 14 shows the ground state energies (1.6 eV) for C_{60}, this time in contact with MoS$_2$ where the electron affinity is about 4.3 eV and the energy gap is 1.35 eV. Vacuum level alignment would obtain the following results: LUMO of C_{60} is well above the CBM of MoS$_2$, while HOMO of C_{60} is nearly equivalent to VBM in the 2H-MoS$_2$ band gap. Because of the larger separation between LUMO of C_{60} and CBM of MoS$_2$, orbital mixing among LUMO and CBM levels would be less than that among the HOMO and VBM levels. However, the local density of states of the C_{60}/2H-MoS$_2$ system near the HOMO energy level may differ from that of the C_{60} and MoS$_2$ due to the weak orbital mixing between the HOMO level of C_{60} and VBM level. 1.6 eV[60],

It indicats that the interactions between the C_{60} and 2H-MoS$_2$(0001) surface are predominantly van de Waals and the electronic structure of the C_{60} film condensed on the 2H-MoS$_2$ is only weakly perturbed due to that in the C_{60} cage, π-electrons are delocalized all over it. This delocalization provides a network of π-electrons which gives C_{60} its static stability.

IV. SUMMARY

The electronic properties and vibrational spectrum of the C_{60} films condensed on the 2H-MoS$_2$(0001) surface have been measured by using XPS, UPS, AES and HREELS. The

electron spectroscopic data of C_{60} films show that the hybridization of the carbon atoms in C_{60} is not strictly in sp^2-bonded state but that the curvature of the molecular surface introduces some $sp^2 p_z$-bonded character into the molecular orbitals. The photoemission data reveal that the valence band spectrum of C_{60} within $10\,eV$ of Fermi level shows a very distinct five-band structure. The surface sensitive HREELS recorded only four strongest vibrational modes in a range of 0–$300\,meV$ at $E_p = 2.0\,eV$, they do not exactly match the four intense infrared band as reported in literatures.

ACKNOWLEDGEMENTS

REFERENCES

[1] H. W. Kroto, J. R. Heath, S. C. O'Brien, R. F. Curl and R. E. Smally, *Nature (London)*, 318(1985), 162.

[2] W. Kratschmer, L. D. Lamb, K. Fostiropoulos, D. R. Huffman, *Nature*, 347(1990), 354.

[3] H. W. Kroto, A. W. Allaf and S. P. Balm, *Chem. Rev.*, 91(1991), 1213.

[4] J. H. Weaver, J. L. Martins, T. Komeda, U. Chen, T. R. Ohno, G. H. Kroll, N. Troullier, R. E. Haufler and R. E. Smalley, *Phys. Rev. Lett.*, 66(1991), 1741.

[5] R. E. Haufler, J. Conceicao, L. P. F. Chibante, Y. Chai, N. E. Byrne, S. Flanagan, M. M. Haley, S. C. O'Brien, C. Pan, Z. Xiao, W. E. Billups, M. A. Ciufolini, R. H. Hauge, J. L. Margrave, L. J. Wilson, R. F. Curi and R. E. Smalley, *J. Phys. Chem.*, 94(1990), 8634.

[6] D. L. Lichtenberger, K. W. Neebesny, C. D. Ray, D. R. Huffman and D. R. Lamb, *Chem. Phys. Lett.*, 176(1991), 203.

[7] R. Tycko, R. C. Haddon, G. Dabbagh, S. H. Glarum, D. C. Douglass and A. M. Mujsce, *J. Phys. Chem.*, 95(1991), 518.

[8] W. Weltner, Jr and R. J. Van Zee, *Chem. Rev.*, 89(1989), 1713.

[9] S. H. Yang, C. L. Pettiette, J. Conceicao, O. Cheshnovsky and R. E. Smally, *Chem. Phys. Lett.*, 139(1987), 233.

[10] H. Ajie, M. M. ALvarez, S. J. Anz, R. D. Beck, F. Diederich, K. Fostiropoulos, D. R. Huffman, W. Kratschmer, Y. Rubin, K. E. Schriver, D. Sensharma and R. L. Whetten, *J. Phys. Chem.*, 94(1990), 8630.

[11] J. H. Weaver, *J. Phys. Chem. Solids*, 53(1992), 1433.

[12] T. R. Ohno, Y. Chen, S. E. Harvey, G. H. Kroll, J. H. Weaver, R. E. Haufler and R. E. Smalley, *Phys. Rev.*, B44(1991), 13747.

[13] T. R. Ohno, Y. Chen, S. E. Harvey, G. H. Kroll, P. J. Benning, J. H. Weaver, L. P. F. Chibante and R. E. Smalley, *Phys. Rev.*, B47(1993), 2389.

[14] M. B. Jost, N. Troullier, D. M. Poirier, J. L. Martins, J. H. Weaver, L. P. F. Chibante and R. E. Smalley, *Phys. Rev.*, B44(1991), 1966.

[15] P. J. Benning, D. M. Poirier, N. Troullier, J. L. Martins, J. H. Weaver, R. E. Haufler, L. P. F. Chibante and R. E. Smalley, *Phys. Rev.*, B44(1991), 1962.

[16] W. M. Tong, D. A. A. Ohiberg, H. K. You, R. S. Williams, S. J. Anz, M. M. Alvarez, R. L. Whetten, Y. Rubin and F. N. Diederich, *J. Phys. Chem.*, 95(1991), 4709.

[17] A. A. Lucas, G. Gensterblum, J. J. Pireaux, P. A. Thiry, R. Candano, J. P. Vigneron, Ph. Lambin and W. Kratschmer, *phys. Rev.*, B45(1992), 13694.

[18] G. Gensterblum, J. J. Pireaux, P. A. Thiry, R. Caudano, J. P. Vigneron, Ph. Lambin A. A. Lucas and W. Kratschmer, *Phys. Rev. Lett.*, 67(1991), 2171.

[19] A. A. Lucas, *J. Phys. Chem. Solids*, 53(1992), 1415.

[20] U. D. Pennino, S. Gozzi, P. Rudolf, P. Lazzeretti, R. Zanasi, C. Taliani, G. Ruani and R. Zamboni, *Proc. 1st Italian workshop on fullerenes.* (1992), p. 125.

[21] A. V. Hamza and M. Balooch, *Chem. Phys. Lett.*, **201**(1993), 404.

[22] G. Gensterblum, L. -M. Yu, J. -J. Pireaux, P. A. Thiry, R. Caudano, J. -M. Themlin, S. Bouzidi, F. Coletti and J. -M. Debever, *Appl. Phys.*, **A56**(1993), 175.

[23] M. Balooch and A. V. Hamza, *Appl. Phys. Lett.*, **63**(1993), 150.

[24] A. Sellidj and B. E. Koel, *J. Phys. Chem.*, **97**(1993), 10076.

[25] S. Modest, S. Cerasari and P. Rudolf, *Phys. Rev. Lett.*, **71**(1993), 2469.

[26] D. K. Kim, Y. D. Suh, K. H. Park, H. P. Noh, S. K. Kim, S. J. Oh and Young Kuk, *J. Vac. Sci. Technol.*, **A11**(1993), 1675.

[27] S. C. Wu, K. Xun, J. Z. Deng, J. Yao, F. Q. Liu, S. H. Lu, Z. Q. Wang, S. R. Han and Z. N. Gu, *Phys. Rev.*, **B47**(1993), 13830.

[28] E. I. Altman and R. J. Colton, *Surf. Sci.*, **279**(1992), 49.

[29] M. Sakurai, H. Tada, K. Saiki and A. Koma, *Jpn, J. Appl. Phys.*, **30**(1991), L1892.

[30] K. Tanigaki, S. Kuroshima, J. Fujita and T. W. Ebbesen, *Appl. Phys. Lett.*, **63**(1993), 2351.

[31] A. Manivannan, H. Hoshi, L. A. Nagahara, Y. Mori, Y. Maruyama, K. Kikuchi, Y. Achiba and A. Fujishima, *Jpn, J. Appl. Phys.*, **31**(1992), 3680.

[32] D. Schmicker, S. Schmidt, J. G. Skofronick, J. P. Toennies and R. Vollmer, *Phys. Rev.*, **B44**(1991), 10995.

[33] W. Krakow, N. M. Rivera, R. A. Roy, R. S. Ruoff and J. J. Cuomo, *J. Mater. Res.*, **7**(1992), 784.

[34] H. G. Busmann, R. Hiss, H. Gaber and I. V. Hertel, *Surf. Sci.*, **289**(1993), 381.

[35] G. Gensterblum, L. M. Yu, J. J. Pireaux, P. A. Thiry, R. Caudano, Ph. Lambin, A. A. Lucas, W. Kratschmer and J. E. Fischer, *J. Phys. Chem. Solids*, **53**(1992), 1427.

[36] J. C. McMenamin and W. E. Spicer, *Phys. Rev.*, **B16**(1977), 5474.

[37] J. P. Coad and J. C. Riviere, *Z. Physik*, **244**(1971), 19; *Surf. Sci.*, **25**(1971), 609.

[38] J. A. Bearden and A. F. Burr, *Rev. Mod. Phys.*, **39**(1967), 125.

[39] P. G. Luire and J. M. Wilson, *Surf. Sci.*, **65**(1977), 476.

[40] G. S. Painter, D. E. Ellis and A. R. Lubinsky, *Phys. Rev.*, **B4**(1971), 3610.

[41] R. F. Willis, B. Fitton and G. S. Painter, *Phys. Rev.*, **B9**(1974), 1926.

[42] C. Kittel, Introduction to Solid State Physics (Wiley, New York, 1971).

[43] R. C. Haddon, *Accts. Chem. Res.*, **25**(1992), 127.

[44] H. Dimigen, H. Hubsch, P. Willich and K. Reiclelt, *Thin solid films*, **129**(1985), 79.

[45] F. R. McFeely, S. P. Kowalczyk, L. Ley, R. G. Cavell, R. A. Pollak and D. A. Shirley, *Phys. Rev.*, **B9**(1974), 5268.

[46] Y. J. Hu, Z. D. Lin, C. H. Wang and K. Xie, *Chin. Phys. Lett.*, **2**(1985), 157; *Acta Phys. Sin.*, **35**(1986), 50 (in Chinese).

[47] J. L. Martins, N. Troullier and J. H. Weaver, *Chem. Phys. Lett.*, **180**(1991), 457.

[48] S. Satpathy, *Chem. Phys. Lett.*, **130**(1986), 545.

[49] R. C. Haddon, L. E. Brus and K. Ragavachari, *Chem. Phys. Lett.*, **125**(1986), 459.

[50] P. A. Bertrand, *Phys. Rev.*, **B44**(1991), 5745.

[51] R. E. Stanton and M. D. Newton, *J. Phys. Chem.*, **92**(1988), 2141.

[52] R. C. Haddon, L. E. Brus and K. Raghavachari, *Chem. Phys. Lett.*, **125**(1986), 459.

[53] D. S. Bethune, G. Meijer, W. C. Tang, H. I. Rosen, W. G. Golden, H. Seki, C. A. Brown and M. S. de Vries, *Chem. Phys. Lett.*, **179**(1991), 181.

[54] J. P. Hare, T. J. Dennis, H. W. Kroto, R. Taylor, A. W. Allaf, S. Balm and D. R. M. Walton, *J. Chem. Soc. Chem. Commun.*, **21**(1991), 412.

[55] D. E. Weeks and W. G. Harter, *J. Chem. Phys.*, **90**(1989), 4744.

[56] B. Chase and P. L. Fagan, *J. Am. Chem. Soc,*, **114**(1992), 2252.

[57] C. Oshima, T. Aizawa, R. Souda, Y. Ishizawa and Y. Sumiyoshi, *Solid State Commun.*, **65**(1988), 1601.

[58] J. C. McMenanin and W. E. Spicer, *Phys. Rev.*, **B16**(1977), 5474.

[59] R. Huisman, R. Dejonge, C. Hass and F. Jellinek, *J. Solid State Chem.*, **3**(1971), 56.

[60] S. H. Yang, C. L. Pettiette, J. Conceicao, O. Cheshnovsky and R. E. Smalley, *Chem. Phys. Lett.*, **139**(1987), 233.